



Trapezoid 2D photonic crystal nanoring resonator-based channel drop filter for WDM systems

R. Rajasekar¹ · S. Robinson²

Received: 14 December 2017 / Accepted: 11 May 2018 / Published online: 8 June 2018
© Springer Science+Business Media, LLC, part of Springer Nature 2018

Abstract

In the present work, a nanostructure of trapezoid photonic crystal ring resonator-based channel drop filter is designed for wavelength division multiplexing systems (WDM) to drop a channel at a center peak wavelength of 1543 nm. The proposed channel drop filter is composed of bus waveguide, drop waveguide, trapezoid nanoring resonator and reflector in a two-dimensional (2D) hexagonal lattice with circular rods arranged in air host. The trapezoid nanoring resonator is playing a very important role in WDM systems for dropping a single channel over a wide wavelength range. The photonic band gaps of perfect lattice structure and non-perfect lattice structure are absolutely calculated by plane wave expansion method. The functional properties of the designed filter are evaluated by finite difference time domain method (FDTD). The functional properties are center peak wavelength, dropping efficiency, passband width and quality factor. The FDTD method results show dropping efficiency is 100%, and quality factor is about 514.33 which are highly suitable for WDM systems. Further, lattice constant, inner and outer rod radius and refractive index difference of the structure are varied to tune the filter center peak wavelength and its corresponding functional parameters effects are investigated. The proposed nanoring resonator-based optical filter is ultra-compact size around $14 \mu\text{m} \times 8.4 \mu\text{m}$; hence, it is extremely suitable for WDM-based photonic communication systems and photonic integrated circuits.

Keywords Photonic crystal · Guided modes · Trapezoid ring resonator · Channel drop filter · Dropping efficiency · Quality factor · WDM systems

1 Introduction

In recent trend, photonic crystal (PC)-based active and passive optical devices are highly attractive and excellent candidates for optical integrated circuits and fiber optic communication systems due to their ultra-compact size, flexible design, very low power, fast response, better lifetime, very low group velocity and more temperature resilient [1]. Generally, the optical filter is one of the outstanding components in WDM-based optical networks and it is used to

accurately select or remove a particular channel wavelength without affecting the remaining channel. Moreover, optical filters also provide numerous advantages, namely very low loss, polarization insensitivity, low temperature-coefficient, high wavelength accuracy, high adjacent channel crosstalk suppression [2]. In recent years, several optical filters are proposed and designed to implement in various optical networks for a variety of applications such as filtering, add/drop functions, and dispersion compensation. The conventional optical filter design is based on Fabry–Perot cavity, fiber Bragg gratings, liquid crystal, microring resonator, array waveguide grating and Mach–Zehnder interferometers [2,3]. Among them, microring resonator is highly attractive due to their wide tunability, flexible mode design, high spectral selectivity and small channel spacing. However, the optical losses, i.e., micro-bending loss and radiation losses, are increased due to reducing the ring size [4]. The above-mentioned issues are overcome by the photonic crystal which provides ultra-low optical loss and strong photon confinement [4]. Photonic crystals (PCs) are dielectric nanostructure with two different

✉ R. Rajasekar
rajasekar8@gmail.com

S. Robinson
mail2robinson@gmail.com

¹ Department of Electronics and Communication Engineering,
Krishnasamy College of Engineering and Technology,
Cuddalore, Tamil Nadu, India

² Department of Electronics and Communication Engineering,
Mount Zion College of Engineering and Technology,
Pudukkottai, Tamil Nadu, India

refractive index materials are arranged in a periodic manner to control the light signal within the structure. The basic property of PC is the photonic band gap (PBG), which make it suitable to control and guide the light signal at the range of optical frequency [1]. The light signal within the PBG frequency range is restricted due to periodicity, the light can be allowed only by removing the periodicity which is executed by creating some defects in the PC structure. Normally, the defects are classified as point, line and surface defect. Basically, PC structures are classified as 1DPC, 2DPC, and 3DPC. The 2DPC has a complete generation of bandgap than 1DPC and provides high speed of operation to execute simulation and fabrication is very easy compared with a 3DPC. For this reason, the 2DPC is preferred for optical filter design [5]. Also, 2DPC best candidate for the optical device due to small size, perfect bandgap computation, strong light confinement, simple structure and easy to incorporate with optical integrated circuits [1]. Recently, 2DPC platform widely used to design the various active and passive optical devices are namely, demultiplexers [5], laser [6], logic gates [7], sensors [8], bandpass filters [9], bandstop filters [10], narrow band filters [11], add-drop filters and channel drop filters [12–25], etc. Especially PC-based channel drop filter (CDF) is highly attractive device for WDM, CWDM, and DWDM-based optical communication systems. So far, PC-based CDFs design is based on nanocavity coupled to waveguides [12], modified L_3 cavities [13] and nanoring resonators [14–25]. Among them, ring resonators provide high performance as it has high dropping efficiency, high-quality factor, low passband width and very low crosstalk.

In the literature, various ring resonator-based optical filters are proposed and designed in square and hexagonal lattice platform. So far, photonic crystal ring resonator (PCRR)-based filters designs are namely, square [14], quasi-square [4, 15], dual-quasi square [16], hexagonal [17], triangular [18], circular [19], X-shaped [20], dual-curved [21], 45° shaped [22], H-shaped [23], flower-shaped [24], curved-Fabry Perot [25] and etc.

In this attempt, a new structure of trapezoid PCRR-based channel drop filter is proposed and designed for WDM system to drop a channel at the center peak wavelength of 1543 nm. The plane wave expansion (PWE) method is used to calculate the lattice constant (a), radius of the rod (R) and refractive index difference (Δ) values, photonic band gap and guided mode of the proposed structure after the defects. The dropping efficiency, quality factor and passband width of the filter are analyzed by FDTD method. Also, filter tuning is achieved by varying the lattice constant, inner and outer radius of the rod and refractive index difference and its corresponding functional parameters also investigated by FDTD method.

The rest of the paper is structured as follows. The PWE method is used to describe the structural parameters, PBG

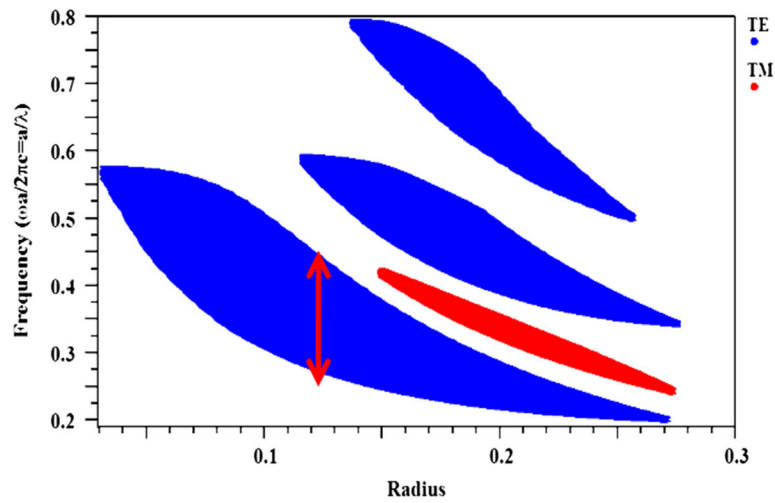
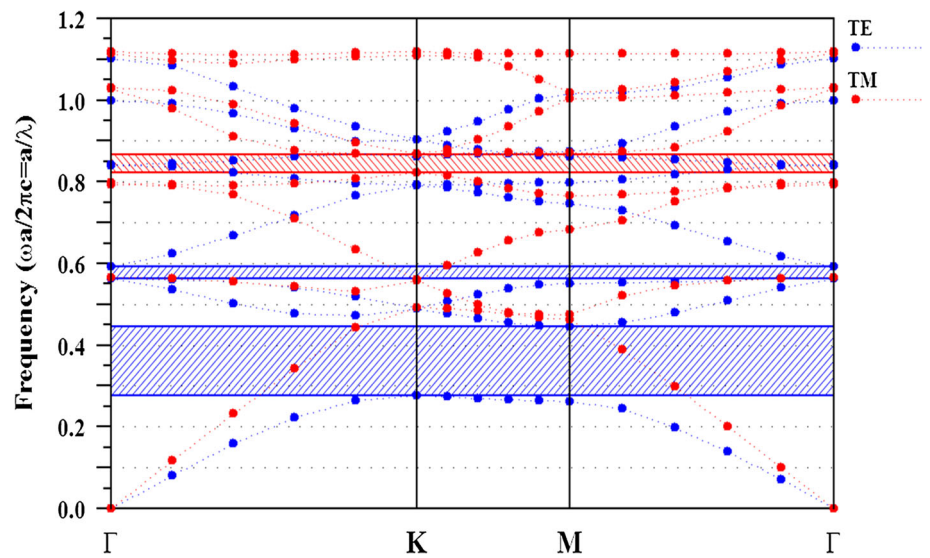
and guided mode which is presented in Sect. 2. The trapezoid PCRR-based CDF design focuses in Sect. 3. FDTD method results are discussed in Sect. 4. Filter tuning and structural parameters are evaluated in Sect. 5. At last, Sect. 6 concludes the paper.

2 Photonic band gap structure

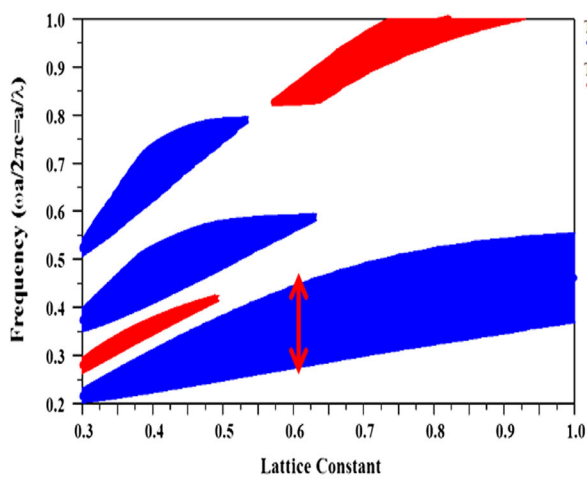
In 2DPCs, the devices can be realized through square lattice or hexagonal lattice and the lattice may be in the form of dielectric rods in air host (rod type) or air holes in a dielectric region (hole type). The hexagonal lattice has large PBG, high filling factor and less sensitive to the incidence angle compared to the square lattice. Moreover, hexagonal lattice acts as a good platform for photonic integrated circuits and easily integrate with other optical devices [26,27]. Hence, authors considered hexagonal lattice. In addition, the proposed CDF design is based on rods in air platform due to their low scattering loss, easy fabrication, low absorption loss, low dispersion loss, and defect-based PC structure effectively produce single mode output [28]. The perfect PC structure composed of 23×16 silicon rods arranged in $X-Z$ directions. The center distance between two adjacent rods is 605 nm which is named as lattice constant (a). The circular rod radius (R) is 121 nm, and the refractive index (n) of the silicon rod is 3.46. The aforementioned structural parameters are used to design the optical filter and obtain the PBG and propagation modes of the periodic and non-periodic structure. There are two PBGs for TE mode and one PBG for TM mode obtained which is shown in Fig. 1. The first TE PBG consider for filter design and its normalized frequency lie between $0.27461 a/\lambda$ to $0.4476 a/\lambda$, i.e., 1351.5–2203.1 nm in terms of wavelength.

In optimizing photonic crystal designs, it is frequently important to characterize the bandgap frequency as a function of design parameters. The good structural parameters of the proposed filter are precisely optimized by using gap map diagrams which are obtained by PWE method. Figure 2a–c shows that the gap map effect for variation of lattice constant, rod radius and delta, respectively. From Fig. 2a, it is clearly noticed that bandgap frequency shifted to lower values while increasing the rod radius in the structure. The optimum value of rod radius is selected as 121 nm and it is highlighted by red line over first TE PBG (blue) region. Alternatively, the PBG frequency shifted to the higher value for lattice constant as shown in Fig. 2b and the best value of lattice constant is selected as 605 nm which is indicated by red line over first TE PBG region. From Fig. 2c, it is clearly observed that the bandgap frequency shifted to the lower values while increasing the delta (refractive index difference) in the structure. The best possible value of delta is selected as 2.46 and it is highlighted by red line over first TE PBG (blue) region. The PBG design in a 2DPC is an important to validate the WDM

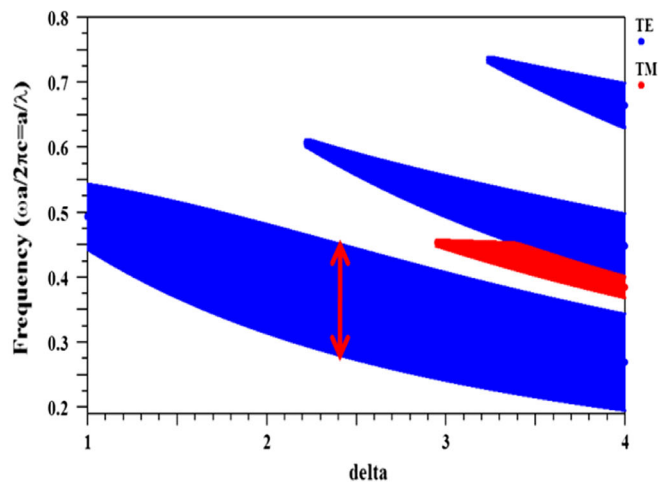
Fig. 1 Band structure of perfect hexagonal lattice structure



(a)



(b)



(c)

Fig. 2 Effect of gap map for hexagonal lattice circular rods for **a** radius, **b** lattice constant and **c** delta

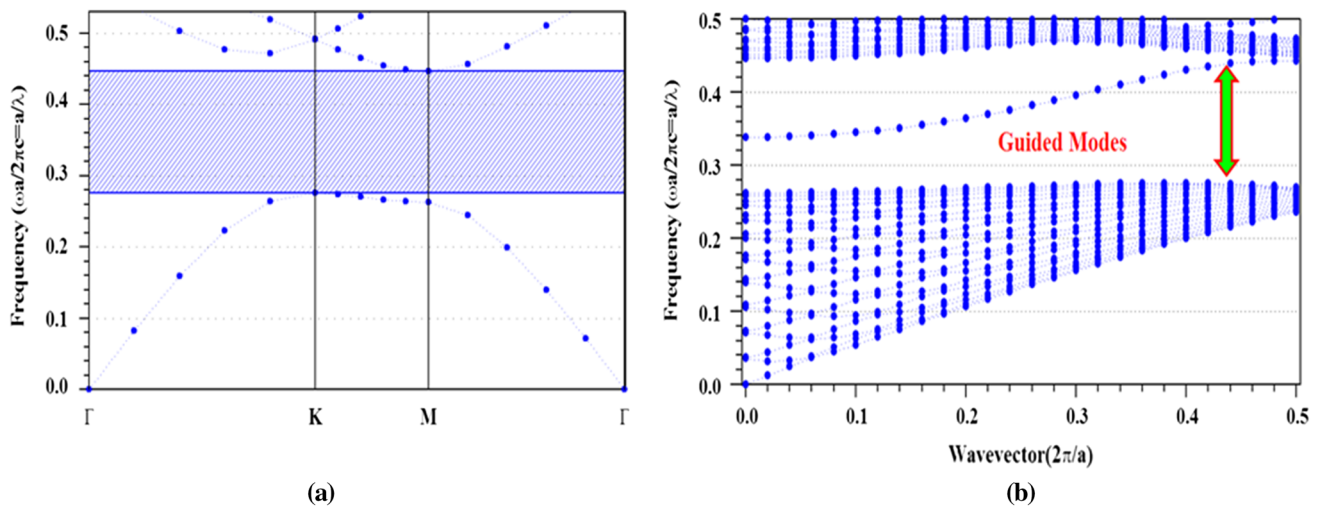


Fig. 3 **a** Band diagram of the proposed device and **b** band diagram after introducing line defects

range of nanophotonic devices when structural parameters changes within it. The size of the PBG is depending upon the value of choosing structural parameters namely lattice constant (a), rod radius (r) and the refractive index difference (Δ). The light signals are propagated through PBG, when it is broken by defects introduced in the structure. The PBG region of the proposed devices before introducing the defects is shown in Fig. 3a. Once the single line defects introduced in the periodic structure, the guided modes are propagated within PBG region as shown in Fig. 3b. From Fig. 3b, it is clearly observed that the guided mode is propagating inside the PBG region over the wavelength lie between 1351.5 and 2203.1 nm in terms of wavelength.

3 Optical ring resonator-based CDF

Figure 4 shows the schematic design of a general channel drop coupled system as composed of two waveguides, namely bus and drop waveguide, coupling element and reflector. Generally, ring resonator acts as a coupling element and play the important role in channel selection from multiplexed input signals. Besides, it has three ports, the port 1 act as input terminal while port 2 and port 3 acts as output terminals which are also termed as through port and drop port, respectively. The WDM signals ($\lambda_1, \lambda_2, \lambda_3, \lambda_4, \lambda_5, \lambda_6, \dots, \lambda_n$) with wide wavelength range is launched from input port to bus waveguide and its confined into coupling element in resonant mode. If the ring resonator supports only one resonant mode, it will decay through both waveguides along the forward and backward directions which introduces the reflection. Hence, in order for complete the transfer to happen, at least two modes are needed for the decaying amplitudes to cancel either the backward direction or the forward direction of the bus waveguide.

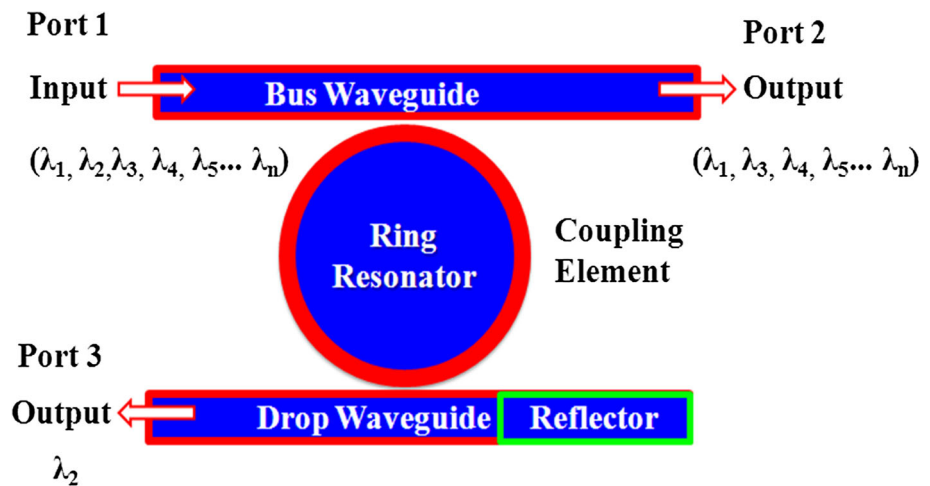
In CDF, at resonance wavelength ($\lambda_2 = 1543$ nm) two localized modes are produce which are named as even mode (λ_2) and odd mode (λ_2). It means that two modes are arrived for a single wavelength (λ_2). The even mode is received in port 3 with same phase (λ_2) and odd mode received in port 2 with out of phase (λ_2). Normally, many of the researchers consider only the port 3 output for CDF design. Generally, CDF drop any one of the wavelength (λ_2) form group wavelength ($\lambda_1, \lambda_2, \lambda_3, \lambda_4, \lambda_5, \lambda_6, \dots, \lambda_n$). For example, in port 3 we assume drop λ_2 channel and remaining all the channel wavelengths are ($\lambda_1, \lambda_3, \lambda_4, \lambda_5, \lambda_6, \dots, \lambda_n$) forwarded to port 2. In port 3, we can drop any one of the aforementioned wavelengths without disturbing other wavelengths [29].

3.1 Photonic crystal ring resonator

Figure 5a shows the proposed PCRR-based CDF. It consists of bus waveguide, drop waveguide, trapezoid PCRR and reflector. The input light signal is transmitted from port ‘I’ and the output signal is reached to the output ports marked as ‘A’ and ‘B’ that is termed as forward transmission and backward direction, respectively. The bus and drop waveguides are formed by line defects. The trapezoid ring resonator is constructed by removing the inner rods in the horizontal direction ($\Gamma-X$) and vertical direction ($\Gamma-Z$). The lower and upper part of the trapezoid PCRR is designed by removing 6 inner rods and 3 inner rods, respectively, in $\Gamma-X$ direction. The left and right side of the trapezoid PCRR is designed by removing the 4 inner rods in $\Gamma-Z$ direction.

The Fig. 5b shows the sectional view of trapezoid nanoring resonator. It consists of coupling rods, scatterer rods, and inner rods. The two rows of coupling rod are located between trapezoid ring resonator and waveguides. The coupling rods are primarily used to couple the light from bus

Fig. 4 Schematic design of the channel drop coupled system



waveguide to ring resonator which in turn ring resonator to drop waveguide at resonance condition. The radius of the coupling rods can influence transmission efficiency and resonant wavelength, therefore eight coupling rods (green color) are shifted in $\Gamma-X$ direction and its radius optimized to 180 nm as a result light energy completely coupled into ring resonator to drop waveguide.

The scatterer rod (S) is placed at the corner of the ring resonator with the radius of 60 nm which is highlighted by black color and it is utilized to minimize the scattering loss and back reflection which leads to improving the performance of the filter. The two rows of 8 inner rods ($R1$) located in the inside of PCRR which is highlighted by dark blue color. Also, inner rod radius changed to 60 nm owing to reducing the nanoring resonator losses which in turn reducing passband width and increase the quality factor. Further, the reflector is located below the right side of the ring resonator, it is used to enhance the dropping efficiency of the filter.

The Fig. 5c clearly shows the 3D view of trapezoid PCRR-based CDF which shows the alignment of silicon pillars in the structure. The total chip area is $14 \mu\text{m} \times 8.4 \mu\text{m}$.

4 Simulation results and discussion

The normalized output response of the proposed optical filter is calculated by using FDTD method. Generally, FDTD method requires correct temporal grid size and time calculations. The Gaussian light signal with TE-like polarization is launched from input port “I” then signal coupled into trapezoid PCRR at a center peak wavelength and its corresponding output detected at output port “B” and remaining signal forward to output port “A”. In both output ports, time monitors are placed to observe the normalized output spectrum which

is calculated by following formula

$$T(f) = \frac{1/2 \int \text{real}(p(f)^{\text{monitor}}) dS}{\text{SourcePower}} \quad (1)$$

where $T(f)$ is the normalized transmission as a function of frequency, $p(f)$ denotes poynting vector and dS is the surface normal. Finally, the $T(f)$ is changed into the function of wavelength. In order to produce a correct simulation, spatial and temporal grid should satisfy the following equation

$$\Delta t \leq \frac{1}{c \sqrt{\frac{1}{\Delta x^2} + \frac{1}{\Delta z^2}}} \quad (2)$$

where Δt is step time, c is the velocity of light in free space and Δx , Δz are space steps along x , z -axes, respectively. Figure 6 shows the normalized output spectra of trapezoid PCRR-based CDF. The center peak wavelength of the CDF is observed at 1543 nm with 100% dropping efficiency and its passband width is 3 nm. The filter performance is calculated by the quality factor (Q) which is defined as the ratio of resonant wavelength to the wavelength change at full width half maximum (FWHM).

$$Q = \frac{\lambda}{\Delta\lambda} \quad (3)$$

where λ is the resonant wavelength and $\Delta\lambda$ is the wavelength difference at FWHM. In this attempt, the trapezoid PCRR-based CDF provides the good quality factor of about 514.33.

The coupling rods are primarily used to couple the light from bus waveguide to ring resonator which in turn ring resonator to drop waveguide at resonance condition. The number of coupling rods (eight) and its values (radius) are properly selected in such a way that to ensure the complete signal transfer from bus waveguide to ring resonator. If the values of coupling rod are not properly selected which

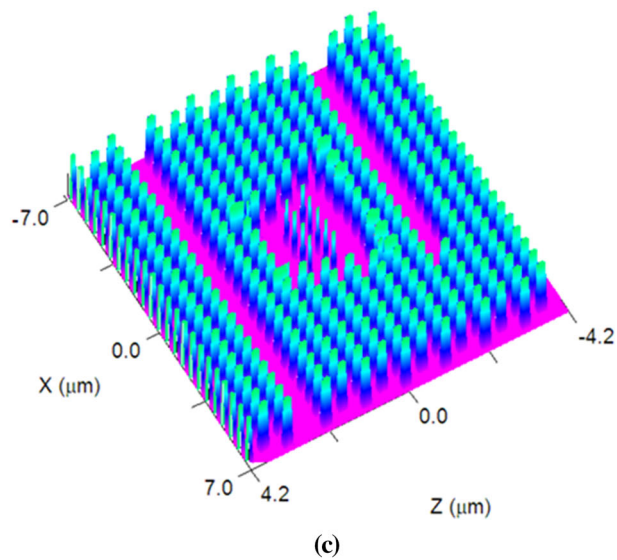
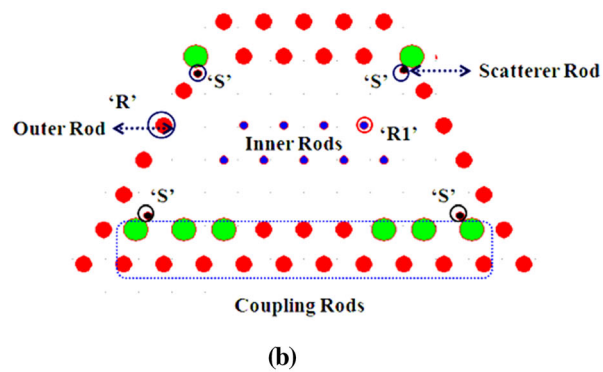
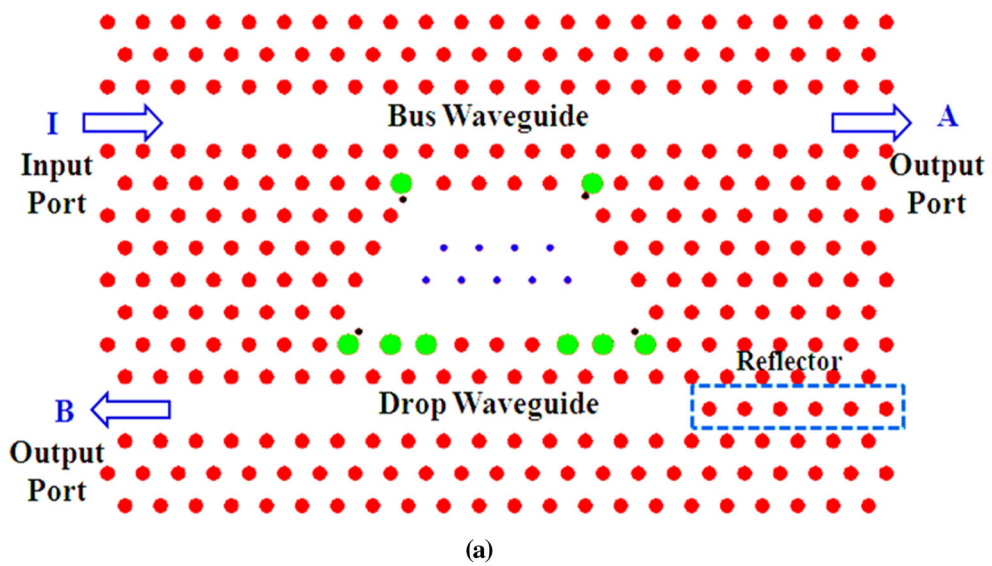
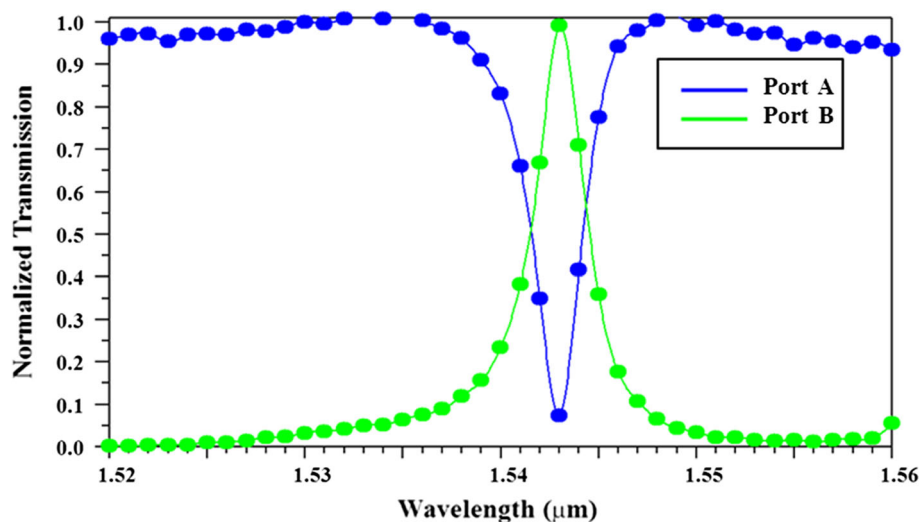


Fig. 5 Trapezoid PCRR-based CDF **a** layout structure, **b** sectional view and **c** three-dimensional (3D) view

Fig. 6 Normalized output spectrum of the PCRR-based CDF



decreases the coupling efficiency, dropping efficiency and other functional parameters. The relation between dimensions of coupling rods (green color) and transmission efficiency is shown in Fig. 7a. From the simulation results, it is clearly observed that, if the coupling rod radius is increased (175–185 nm), the resonant wavelength is red shifted and transmission efficiency is also varied. The coupling rods radius of 180 nm shows high transmission efficiency (100%) compared to 175 nm (86.6%) and 185 nm (76%) coupling rod radius. Hence, 180 nm of coupling rod radius is accounted in this work. In addition, the rods other than coupling rod are used to provide mechanical strength of the structure and increase the confinement of the signal.

The coupling rod rows are increased to enhance the quality factor; however, transmission efficiency is reduced. The impact of normalized transmission with respect to the coupling rod effect with and without optimization is shown in Fig. 7b. The simulation results clearly shows that without optimization of coupling rods, the transmission efficiency is very low about 11%, as a very less amount of light signal coupled into ring resonator to drop waveguide. However, with optimization of eight coupling rods (green color) are used to enhance the transmission efficiency (100%) which means that light signal completely coupled into ring resonator to drop waveguide. From the simulation result, it is observed that after the optimization of coupling rods, the transmission efficiency is increased significantly. Hence, reference rods (red color) are used to couple the small amount of light while optimized coupling rods (green color) are used to couple more amount of light within ring resonator.

Figure 8 shows the normalized output spectrum of the ring resonator-based CDF without and with scatterer rod. The simulation result clearly shows that the dropping efficiency (78.38%), and quality factor (428.33) of the CDF without

scatterer rods become low due to the backward and scattering loss are produced at corners at the center peak wavelength.

Figure 9a clearly shows at a center peak wavelength 1543 nm the electric field of input light signal is completely (100%) coupled with nanoring resonator and dropped into its output port B, which is termed as on resonance. However, at off-resonance 1555 nm, the electric field energy is directly forwarded to output port A and also observed that due to scattering loss small amount of signal power (1–8% is negligible) is coupled into ring resonator as shown in Fig. 9b.

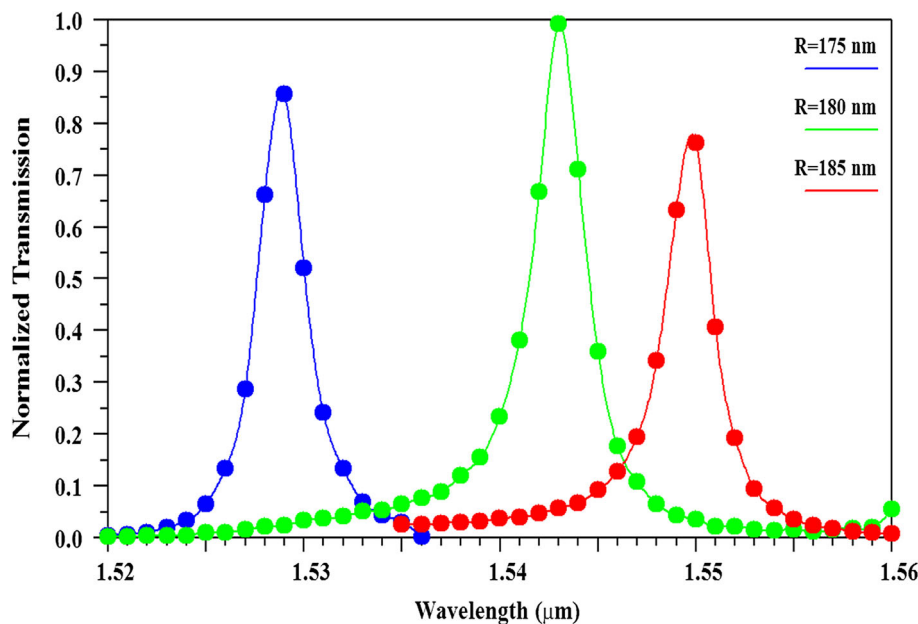
5 Tunability in proposed CDF

Recent years, data transmission through ultra-high-speed optical network path is highly congested due to the huge amount of information which have been used for various real-time applications such as High-Definition Television (HDTV), Video-on-Demand (VoD), Voice-over-IP (VoIP) and high-speed Internet. Therefore, the cumulative optical network bandwidth is greatly enhanced by multiple channel wavelengths that are simultaneously transmitted over a single fiber. The ultra-small photonic component of CDF filter is the attractive candidate which is used to select a single channel from the multi-wavelength network with very low crosstalk. Typically, the ring resonator-based CDFs are used but it operates at a fixed wavelength. However, PCRR-based optical filter can be effectively tuned by different tuning mechanisms.

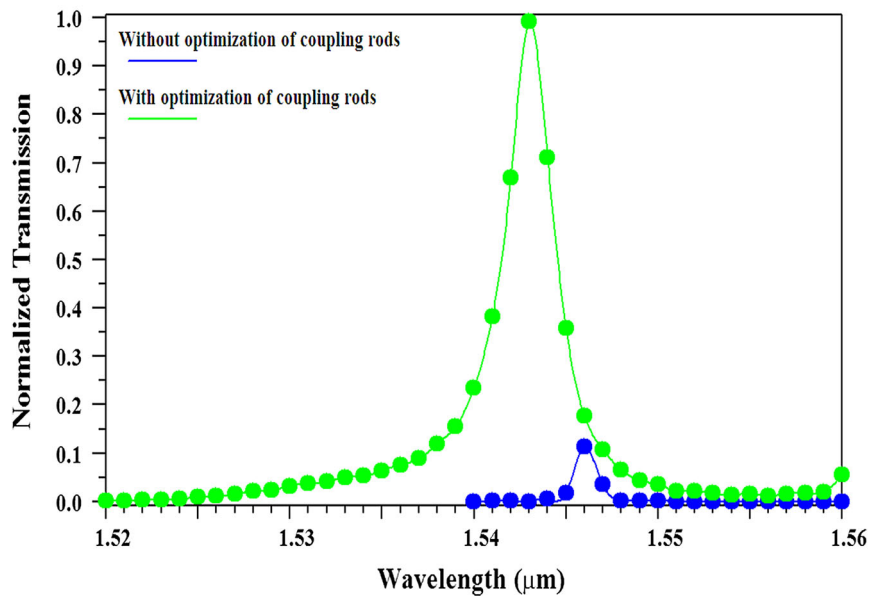
5.1 CDF tuning mechanisms

Generally, PC tunability executed by two different mechanisms such as PC tuning within itself and PC tuning without itself. In the first mechanism to modify both structural geom-

Fig. 7 Normalized output spectrum of the PCRR-based CDF **a** at different coupling rod radius and **b** without and with optimization of coupling rods



(a)



(b)

etry (a, r) and material characteristics (μ or n). In second mechanism dynamic material (liquid or solid) including into PC structure which is highly sensitive to external excitation. The aforementioned tuning mechanisms are used to realize filter tuning and effectively shifting the resonant wavelength over the wide wavelength range. The five different methods are extensively used for photonic crystal tuning namely, structural tuning, thermal tuning, electrical tuning, magnetic tuning, and mechanical tuning [30]. All the aforementioned tuning mechanisms have some pros and cons. Among them, structural tuning method is very simple and does not affect

the optical filter performance [19]. Hence, structural parameter ($a, R, R1$ and δ) tuning is considered in this paper, as a result, four different cases are considered for filter tuning. Generally, in PC-based device, if the lattice constant, radius of the rod and refractive index of the rod is varied whose corresponding resonant wavelength is varied linearly based on the amount of value change in the structural parameters. As the PBG region is varied owing to the change of structural parameters which in turn change in resonant wavelength shift. If the structural parameter value is increased, the PBG region is shifted into the higher wavelength region; therefore,

Fig. 8 Normalized output spectrum of the PCRR-based CDF without and with scatterer rod

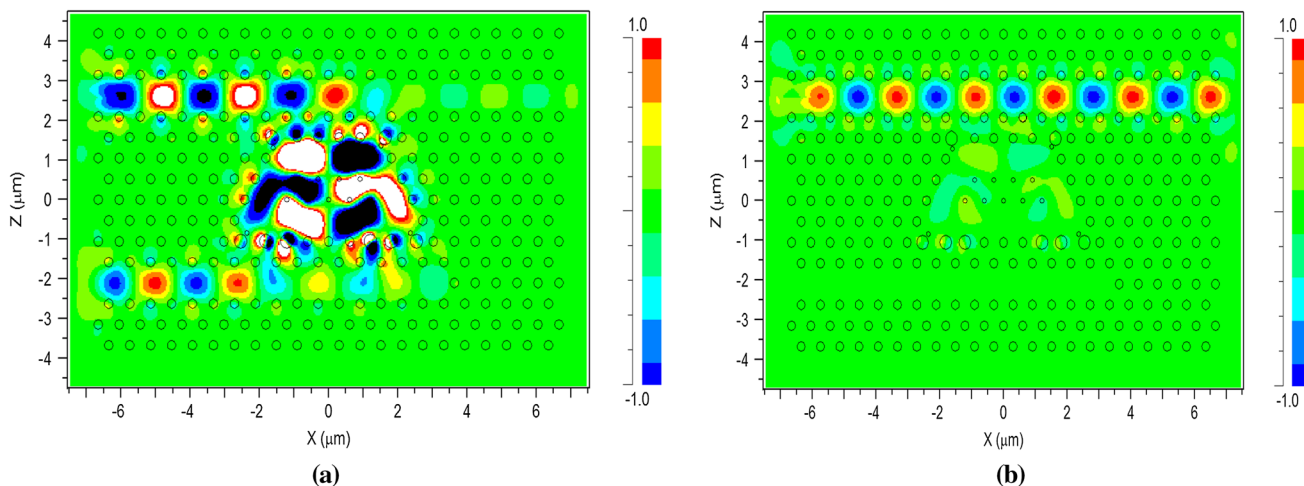
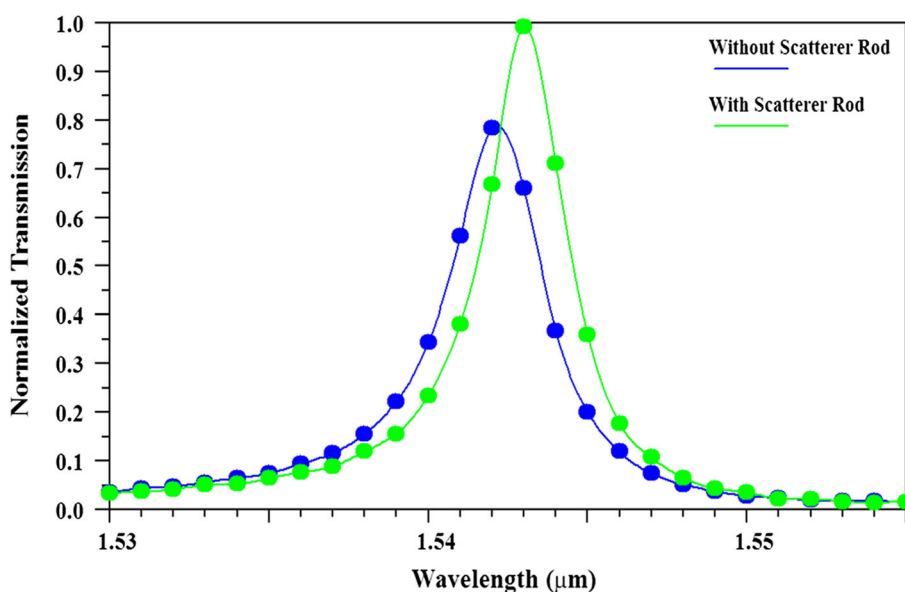


Fig. 9 Electric field distribution of trapezoid ring resonator at **a** 1543 nm and **b** 1555 nm

the resonant wavelength is shifted into the higher wavelength region and vice versa.

5.2 Lattice constant tuning

The first case, the lattice constant of the structure is varied with an increment of 1 nm from 604 to 606 nm and its corresponding normalized output spectrum is investigated which is shown in Fig. 10a. From the simulation results, it is observed that the center peak wavelength of the CDF is linearly shifted to higher wavelength and its dropping efficiency and quality factor slightly increased but passband width remain constant. The functional parameters of CDFs are compared with different lattice constants are tabulated in Table 1. Further, CDF is used to detect the minute lattice constant variation of 0.3 nm (605.3 nm) and its center peak

wavelength has shifted by 0.7 nm compared with a reference value (605 nm) which is shown in Fig. 10b. The lattice constant sensitivity (S_a) is calculated by the following equation.

$$S_a = \frac{\Delta\lambda}{\Delta a} \tag{4}$$

where $\Delta\lambda$ represents the resonant wavelength difference and Δa represents the lattice constant difference. The obtained result shows that lattice constant sensitivity is equal to 2.33, hence the small lattice constant variation is highly sensitive to resonant wavelength tuning.

5.3 Radius of the rod tuning

The second case, the outer and inner rod radius of the ring resonator is modified from 111 to 133 nm and 59 to 61 nm

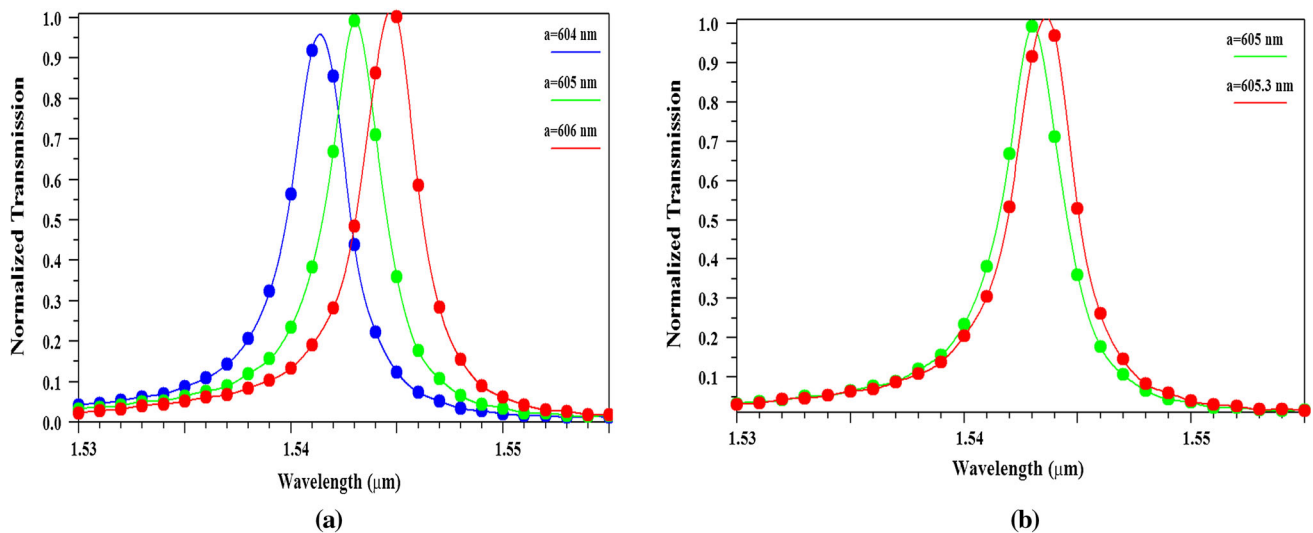


Fig. 10 Normalized output spectrum of the PCRR-based CDF at **a** different lattice constant and **b** minute lattice constant variation

Table 1 The functional parameters of the CDF at different lattice constant

Lattice constant (nm)	Resonant wavelength (nm)	Transmission efficiency (%)	Passband width (nm)	Quality factor
604	1541.3	95.6	3	513.76
605	1543.0	100	3	514.33
606	1544.8	100	3	514.93
605.3	1543.7	100	3	514.56

with the step of 1 nm and its normalized transmission spectrum is shown in Fig. 11a, b. The numerical result shows that resonant wavelength of the optical filter is highly sensitive to inner rod radius ($R1$) compare to outer rod radius (R). As a result, outer rod radius is more resilient to wavelength tuning compared to inner rod radius. Also, abrupt changes in dropping efficiency and quality factor are observed while changing the outer rod radius. However inner rod radius tuning, dropping efficiency and quality factor is trivial change with high linearity. The functional parameters of CDFs are compared with different inner rods radius and are tabulated in Table 2. Moreover, optical filter is used to detect the small inner rod variation of 0.5 nm (60.5 nm) and its center peak wavelength has shifted by 1 nm compared with the reference value (60 nm) which is shown Fig. 11c. The inner rod radius sensitivity (S_r) is calculated by the following equation.

$$S_r = \frac{\Delta\lambda}{\Delta R1} \tag{5}$$

where $\Delta\lambda$ represents the resonant wavelength difference and $\Delta R1$ represents the inner rod radius difference. The obtained result shows that rod radius sensitivity is equal to 2; therefore, small inner rod radius is highly sensitivity to resonant wavelength tuning.

5.4 Effect of variation in filling fraction

The radius of the rod is directly influenced in the filling fraction of the structure which is defined as the rods occupied area in the hexagonal lattice. The filter design is based on circular rods in hexagonal lattice, the single circular rod area in the PC structure is calculated by using the basic formula (πr^2). The perfect PC platform composed 368 (23×16) rods in a hexagonal lattice and after line and point defects are introduced to remove 56 rods in vertical and horizontal direction, therefore, after creating the defects total number of rods in PC platform is 312, however 8 coupling rods (180 nm) and 9 inner rods (60 nm) radius is increased form reference value owing to increase the filter performance. Hence, the total number rod in the PC structure is 295 ($312 - 8 - 9 = 295$) which is collectively named as outer rods. The scattering and back reflection is reduced by inserting the 4 rods at the corner of the trapezoid ring resonator structure. Finally, the total number of rods in the proposed structure is equal to 316 ($295 + 8 + 9 + 4$). The four different single rod area is calculated and then it multiplies by the corresponding total number of rods to obtain the individual filling fraction. The cumulative filling fraction is calculated by adding four different rod individual filling fraction and it is clearly shown in Table 3.

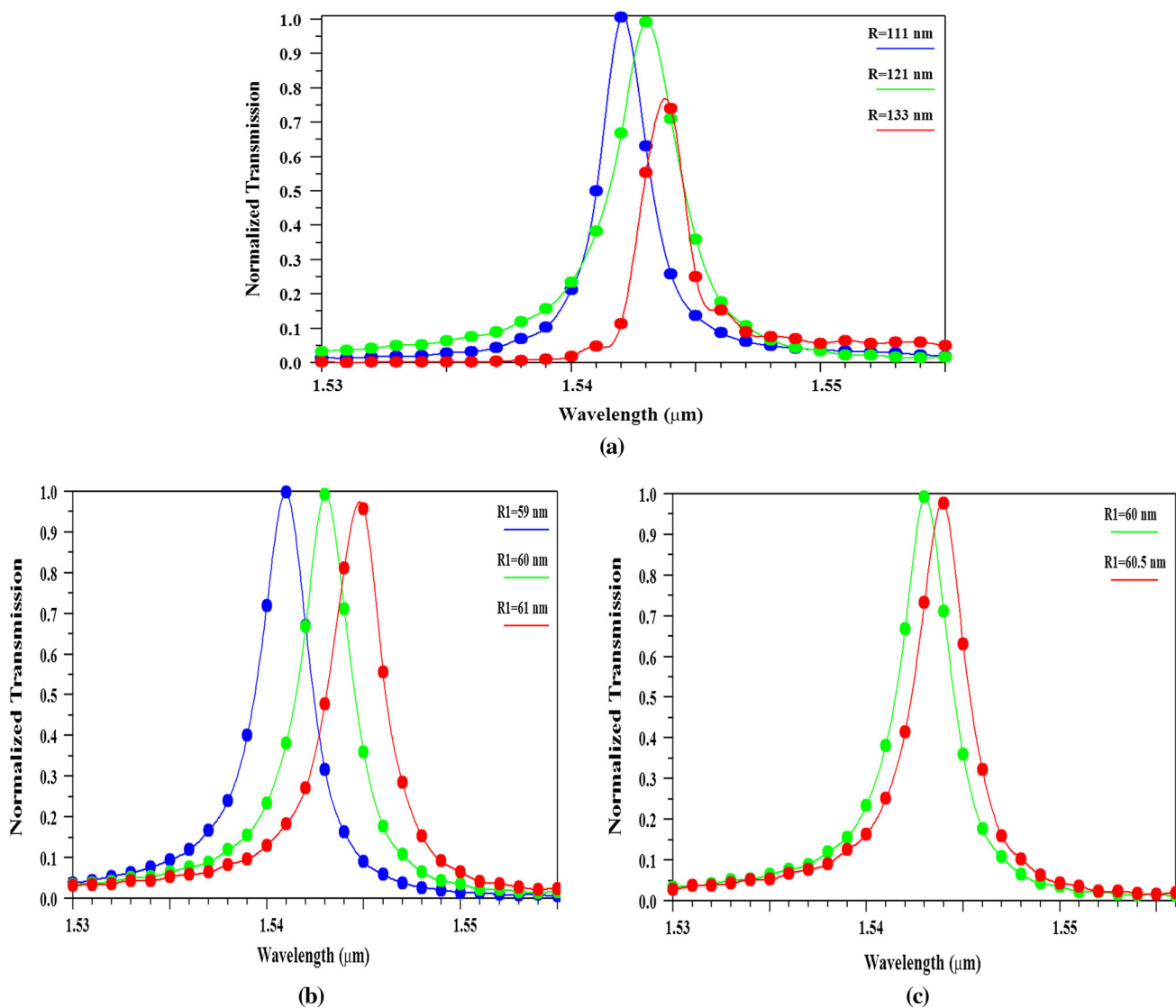


Fig. 11 Normalized output spectrum of the PCRR-based CDF at **a** different outer rod radius, **b** different inner rod radius and **c** minute inner rod variation

Table 2 The functional parameters of the CDF at different inner rod radius

Inner rod radius (<i>R</i> 1) (nm)	Resonant wavelength (nm)	Transmission efficiency (%)	Passband width (nm)	Quality factor
59	1541.0	100	3	513.66
60	1543.0	100	3	514.33
61	1544.9	97.2	3	514.96
60.5	1544.0	97.8	3	514.66

To study the impact of center peak wavelength with reference to cumulative filling fraction, the inner rod radius changed from 59 to 61 nm with an increment of 0.5 nm. The variation in cumulative filling fraction while changing the radius is $13.765 \times 10^{-12} \text{ m}^2$ to $13.772 \times 10^{-12} \text{ m}^2$ and its equivalent center peak wavelength varied from 1541 to 1544.9 nm. From the simulation results clearly observed

that 1 nm center peak wavelength linearly shifted to higher wavelength while changing the inner rod radius which leads to increase the filling fraction. Figure 12 shows the linear relationship between cumulative filling fraction and resonant wavelength. The CDF functional parameters such as dropping efficiency and quality factor slightly changed at higher filling traction which are listed in Table 4.

Table 3 Filling fraction calculation of single and total number of rods in a hexagonal lattice

Different type of rod	Total number of rods	Rod radius (nm)	Single rod area (m ²)	Filling fraction (with defects) (m ²)	Hexagonal lattice area (m ²)	Filling fraction (%)
Outer rods	295	121	0.04590×10^{-12}	13.5405×10^{-12}	117.6×10^{-12}	11.7080
Coupling rods	8	180	0.01017×10^{-12}	0.08136×10^{-12}		
Scatterer rods	4	60	0.01130×10^{-12}	0.04520×10^{-12}		
Inner rods	9	60	0.01130×10^{-12}	0.10170×10^{-12}		
Total no. of rods	316			13.7687×10^{-12}		

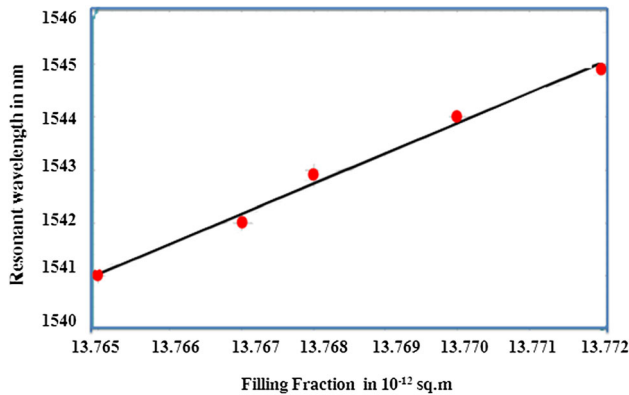


Fig. 12 Effect of resonant wavelength variation in filling fraction

5.5 Refractive index difference tuning

The third case, the refractive index difference (Δ) is varied with an increment of 0.01 from 2.45 to 2.47 and its corresponding normalized output spectrum is shown in Fig. 13a. The center peak wavelength of the CDF is linearly shifted to higher wavelength and its dropping efficiency and quality factor trivial changes are observed. The functional parameters of CDFs are compared with different refractive index difference and are tabulated in Table 5.

Further, the optical filter is used to detect the small refractive index variation of 0.003 (2.463) and its center peak wavelength has shifted by 0.8 nm compared with the reference value (2.46) which is shown in Fig. 13b. The refractive index difference sensitivity (S_n) is calculated by the following equation.

$$S_n = \frac{\Delta\lambda}{\Delta n} \tag{6}$$

where $\Delta\lambda$ represents the resonant wavelength difference and Δn represents the refractive index difference. The obtained result shows that refractive sensitivity is 266.66 nm/RIU, as a result, refractive index difference is highly sensitivity to resonant wavelength tuning and this value is highly suitable for WDM systems and nanosensor applications.

5.6 Cumulative structural parameters tuning

The high-resonant wavelength tuning is normally obtained by changing all the structural parameters, for this reason simultaneously varied all the three parameters as an alternative of varying any one of the parameters such as lattice constant, inner radius of the rod and refractive index difference. These three parameters are collectively named as cumulative structural parameters (CS) and its different combinations are used to obtain the high-resonant wavelength tuning as shown in Fig. 14a. For CS-1 tuning, center peak wavelength 5 nm (1538 nm) shifted to the lower wavelength from the center peak wavelength of 1543 nm. For CS-3 tuning, center peak wavelength 5.6 nm shifted to the higher wavelength from the center peak wavelength of 1543 nm. The lower and higher wavelength shifting is obtained owing to the cumulative dielectric strength of the PCRR is reduced and increased, respectively. The functional parameters of CDFs are compared with different CS values and are tabulated in Table 6. For CS-4 tuning there is 2 nm center peak wavelength shift is

Table 4 Filling fraction, resonant wavelength and transmission efficiency at different rod radius

Inner rod radius (nm)	Filling fraction (m ²)	Filling fraction (%)	Resonant wavelength (nm)	Transmission efficiency (%)
59.0	13.765×10^{-12}	11.705	1541.0	100
59.5	13.767×10^{-12}	11.706	1542.0	100
60.0	13.768×10^{-12}	11.707	1543.0	100
60.5	13.770×10^{-12}	11.709	1544.0	97.8
61.0	13.772×10^{-12}	11.710	1544.9	97.2

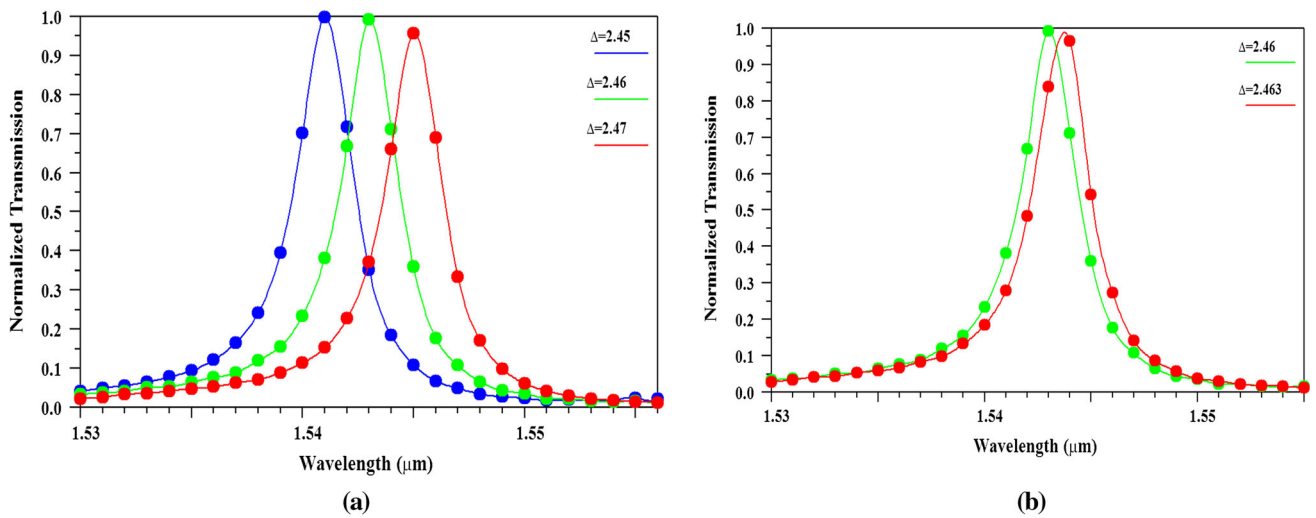


Fig. 13 Normalized output spectrum of the PCRR-based CDF at **a** different refractive index difference and **b** minute refractive index variation

Table 5 The functional parameters of the CDF at different refractive index difference

Refractive index difference (RIU)	Resonant wavelength (nm)	Transmission efficiency (%)	Passband width (nm)	Quality factor
2.45	1541.0	100	3	513.66
2.46	1543.0	100	3	514.33
2.47	1545.0	96.4	3	515.00
2.463	1543.8	98.32	3	514.60

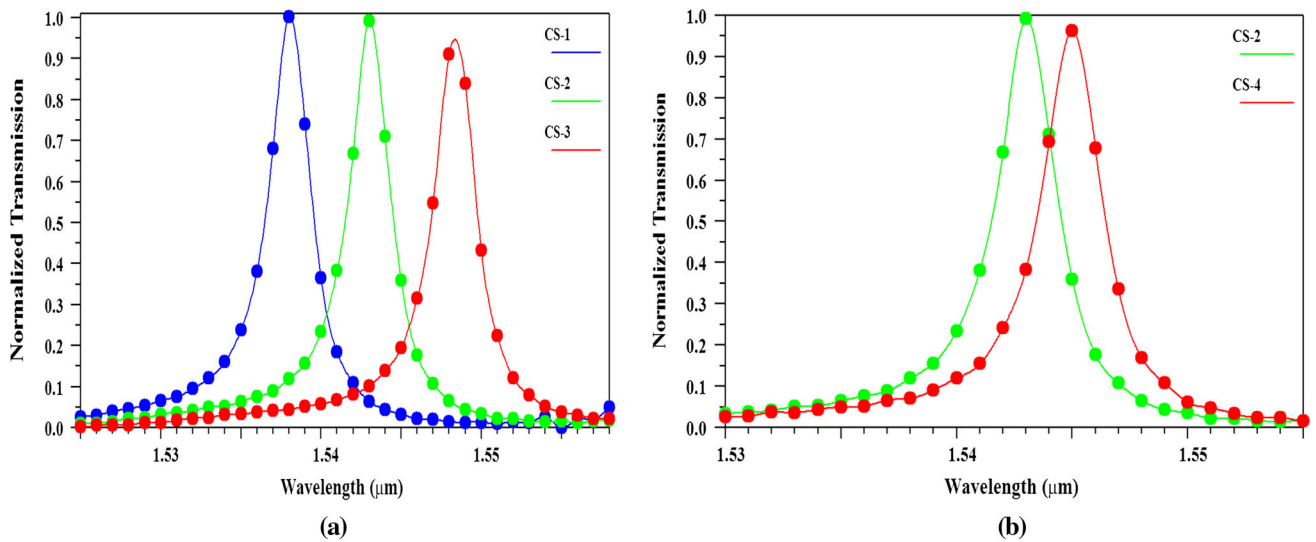


Fig. 14 Normalized output spectrum of the PCRR-based CDF at **a** different cumulative structural parameter and **b** minute cumulative structural parameter variation

Table 6 The functional parameters of the CDF at different cumulative structural parameters

Cumulative structural parameter (CS)		Resonant wavelength (nm)	Transmission efficiency (%)	Passband width (nm)	Quality factor
CS-1	$a = 604, R1 = 59$ and $\Delta = 2.45$	1538.0	100	3	512.66
CS-2	$a = 605, R1 = 60$ and $\Delta = 2.46$	1543.0	100	3	514.33
CS-3	$a = 606, R1 = 61$ and $\Delta = 2.47$	1548.6	94.5	3	516.20
CS-4	$a = 605.3, R1 = 60.5$ and $\Delta = 2.463$	1545.0	96.1	3	515.00

Table 7 Comparison of designed PCRR filter with the existed PCRR-based filter

Reference	Lattice structure	Dimension (μm^2)	Type of PCRR cavity	Dropping efficiency (%)	Passband width (nm)	Quality factor
[4]	Square	***	Quasi-square	96.0	9.80	160.0
[14]	Square	189.6	Square shaped	35.5	3.50	437.7
[15]	Square	242.4	Quasi-square	90	4.00	387
[16]	Square	174.1	Dual-quasi-square	89.0	3.50	399.0
[17]	Triangular	***	Hexagonal shaped	55.0	3.69	423.0
[18]	Triangular	315	Triangular shaped	100	4.00	377.5
[19]	Square	129.9	Circular shaped	100	13.0	114.6
[20]	Triangular	***	X-shaped	100	7.90	196.0
[21]	Triangular	***	Dual curve shaped	68.0	9.80	153.6
[22]	Square	***	45° shaped	90.0	1.85	840.0
[23]	Square	***	H-shaped	100	7.01	221.0
[24]	Square	152.7	Flower shaped	100	8.0	205.5
[25]	Square	123.0	Curved Fabry–Perot	99.0	13.0	192.0
Present work	Triangular	117.6	Trapezoid shaped	100	3.00	514.3

***Not discussed

observed while at once minutely varying the lattice constant, inner radius of the rod, refractive index difference by 0.3 nm, 0.5 nm, and 0.003, respectively, from the constant value and its corresponding result shown in Fig. 14b.

The passband width directly proportional to energy loss in the cavity (ring resonator). The trapezoid ring resonator energy loss is mainly based on the inner rod radius; therefore, passband width remains constant for small inner rod radius (every 0.01 nm increment) variation. In addition, lattice constant (every 1 nm increment) and refractive index (every 0.01 RIU increment) value slightly changed which does not affect the energy loss within the ring resonator which leads to provide constant passband width.

The PCRR-based optical filter functional parameters namely device dimension, cavity type, dropping efficiency, passband width and quality factor are compared with the reported PCRR-based optical filters which are listed in Table 7. From this table, observed that curved Fabry–Perot resonator is designed with small dimension is 123.0 μm^2 and

high dropping efficiency (99%) however passband width is very high and Q factor is very low. However, 45° shaped PCRR cavity provides low passband width is 1.8 nm and high Q factor is 840; however, it provides 90% transmission efficiency. Meanwhile, triangular, circular, H-shape and flower-shaped PCRR cavity were used to provide 100% dropping efficiency; however, passband width and Q factor are very low. From this analysis, it is clear that the proposed trapezoid PCRR-based CDF provides enhanced result in all aspects.

6 Conclusions

The trapezoid ring resonator-based CDF is designed using the hexagonal lattice platform to drop a channel at a center peak wavelength of 1543 nm. The FDTD results show 100% of dropping efficiency is observed at 1543 nm and its passband width is 3 nm and quality factor is about 514.33 which is

the higher value compared to the reported CDFs. The center peak wavelength tuning of nanoring resonator-based CDF is numerically investigated by changing the structural parameters individually and simultaneously and its corresponding functional parameters are also analyzed. From the simulation result, for every 0.3 nm variations in lattice constant, 0.5 nm variations in the inner rod radius and 0.003 variations in refractive index difference, there is 0.7 nm, 1 nm and 0.8 nm center peak wavelength shift observed. The designed CDF is ultra-compact and total chip area is $14 \mu\text{m} \times 8.4 \mu\text{m}$. Hence, this type of device is highly suitable for the realization of photonic integrated circuits for WDM systems and nanochip-based sensing applications.

References

- [1] Joannopoulos, J.D., Meade, R.D., Winn, J.N.: *Photonic Crystals-Molding the Flow of Light*. Princeton University Press, Princeton (1995)
- [2] Ramaswami, R., Sivarajan, K.N., Sasaki, G.H.: *Optical Networks*, 3rd edn. Morgan Kaufmann Publishers, Burlington (2010)
- [3] Sadot, D., Boimvich, E.: Tunable optical filters for dense WDM networks. *IEEE Commun. Mag.* **36**, 50–55 (1998)
- [4] Qiang, Z., Zhou, W., Soref, R.A.: Optical add-drop filters based on photonic crystal ring resonators. *Opt. Express* **15**(4), 1823–1831 (2007)
- [5] Venkatachalam, K., Robinson, S., Dhamodharan, S.K.: Performance analysis of an eight channel demultiplexer using a 2D-photonic crystal quasi square ring resonator. *Opto-Electron. Rev.* **25**, 74–79 (2017)
- [6] Cao, D., Tandaechanurat, A., Nakayama, S., Ishida, S., Iwamoto, S., Arakawa, Y.: Silicon-based three-dimensional photonic crystal nanocavity laser with InAs quantum-dot gain. *Appl. Phys. Lett.* **101**, 191107 (2012)
- [7] Salmanpour, A., Mohammadnejad, S., Bahrami, A.: Photonic crystal logic gates an overview. *Opt. Quantum Electron.* **47**(7), 2249–2275 (2015)
- [8] Zhang, Y., Zhao, Y., Lv, R.: A review for optical sensors based on photonic crystal cavities. *Sens. Actuators A Phys.* **233**, 374–389 (2015)
- [9] Robinson, S., Nakkeeran, R.: Investigation on two dimensional photonic crystal resonant cavity based bandpass filter. *Optik* **123**, 451–457 (2011)
- [10] Robinson, S., Nakkeeran, R.: Bandstop filter for photonic integrated circuits using photonic crystal with circular ring resonator. *J. Nanophotonics* **5**, 053521 (2011)
- [11] Lu, Y., Liu, H., Sun, Q., Huang, N., Wang, Z.: Terahertz narrow-band filter based on rectangle photonic crystal. *J. Mod. Opt.* **63**, 224–230 (2015)
- [12] Feng, S., Wang, Y.: Tunable multichannel drop filters based on the two-dimensional photonic crystal with oval defects. *Optik* **123**, 688–691 (2012)
- [13] D'souza, N.M., Mathew, V.: Two dimensional tunable photonic crystal defect based drop filter at communication wavelength. *Photonics Nanostruct. Fundam. Appl.* **25**, 14–18 (2017)
- [14] Sathyadevaki, R., Sivanantharaja, A., Shanmuga sundar, D.: Photonic crystal-based optical filter: a brief investigation. *Photonic Netw. Commun.* **33**(1), 77–84 (2016)
- [15] Alipour-Banaei, H., Jahanara, M., Mehdizadeh, F.: T-shaped channel drop filter based on photonic crystal ring resonator. *Optik* **125**(18), 5348–5351 (2014)
- [16] Niyazi, M., Amirkhani, A., Mosavi, M.R.: Investigation and simulation of a two-channel drop filter with tunable double optical resonators. *J. Supercond. Nov. Magn.* **27**, 827–834 (2014)
- [17] Hsiao, F.L., Lee, C.: A nano-ring resonator based on 2-hexagonal-lattice photonic crystals. In: *IEEE/LEOS International Conference on Optical MEMS and Nanophotonics*, pp. 107–108 (2009)
- [18] Rajalakshmi, G., Sivanantharaja, A., Shanmuga sundar, D.: Design and optimization of two dimensional photonic crystal based optical filter. *J. Nonlinear Opt. Phys. Mater.* **24**(3), 1550027 (2015)
- [19] Robinson, S., Nakkeeran, R.: Two dimensional photonic crystal ring resonator based add drop filter for CWDM systems. *Optik* **124**, 3430–3435 (2013)
- [20] Mahmoud, M.Y., Bassou, G., Taalbi, A., Chekroun, Z.M.: Optical channel drop filters based on photonic crystal ring resonators. *Opt. Commun.* **285**, 368–372 (2012)
- [21] Andalib, P., Granpayeh, N.: Optical add/drop filter based on dual curved photonic crystal resonator. In: *IEEE/LEOS International Conference on Optical MEMS and Nanophotonics* (2008)
- [22] Bai, J.B., Wang, J.Q., Chen, X.Y., Jiang, J.Z., Li, H., Qiu, Y.S., Qiang, Z.X.: Characteristics of 45° photonic crystal ring resonators based on square-lattice silicon rods. *Optoelectron. Lett.* **6**, 203–206 (2010)
- [23] Rezaee, S., Zavvari, M., Alipour-Banaei, H.: A novel optical filter based on H-shape photonic crystal ring resonators. *Optik* **126**(20), 2535–2538 (2015)
- [24] Rashki, Z., Seyyed Mahdavi Chabok, S.J.: Novel design of optical channel drop filters based on two-dimensional photonic crystal ring resonators. *Opt. Commun.* **395**, 231–235 (2017)
- [25] Chhipa, M.K., Radhouene, M., Dikshit, A., Robinson, S., Suthar, B.: Novel compact optical channel drop filter for CWDM optical network applications. *Int. J. Photonics Opt. Technol.* **2**(4), 26–29 (2016)
- [26] Jamois, C., Wehrspohn, R., Schilling, J., Muller, F., Hillebrand, R., Hergert, W.: Silicon-based photonic crystal slabs: two concepts. *IEEE J. Quantum Electron.* **38**, 805–810 (2002)
- [27] Matthews, A., Wang, X.-H., Kivshar, Y., Gu, M.: Band-gap properties of two-dimensional low-index photonic crystals. *Appl. Phys. B* **81**, 189–192 (2005)
- [28] Kok, A.A.M., Vander Tol, J.J.G.M., Roel, B., Smit, M.K.: Reduction of propagation loss in pillar-based photonic crystal waveguides. *J. Lightwave Technol.* **27**, 3904–3911 (2009)
- [29] Fan, S., Villeneuve, P.R., Joannopoulos, J.D., Haus, H.A.: Channel drop tunneling through localized states. *Phys. Rev. Lett.* **80**(5), 950–963 (1998)
- [30] Zhao, Y., Ying, Y., Wang, Q.: Latest research progress on methods and technologies for tunable photonic crystals. *Opt. Laser Technol.* **64**, 278–287 (2014)



R. Rajasekar was born in Tamilnadu, India, in 1986. He received B.E. degree in Electronics and Communication Engineering from Anna University, Tamilnadu, India, and M.E. degree in Optical Communication from Alagappa-Chettiar College of Engineering and Technology, Karaikudi, Tamilnadu, India, in 2007 and 2010, respectively. He is currently working as Assistant Professor, Department of Electronics and Communication Engineering, Krishnasamy College of Engineering and Technology, Cuddalore, Tamil Nadu, India. He is a life member of ISTE. He attended 15 workshops and organized 10 programmes. His current research interests are in the areas of Opti-

cal Communication, Photonic Crystals, Photonic Integrated Circuits, Nano-Optical Devices and Optical Networks.



S. Robinson was born in Tamilnadu, India, in 1982. He received B.E. degree in Electronics and Communication Engineering from Bharathidasan University, Tamilnadu, India, and M.E. degree in Optical Communication from Alagappa Chettiar College of Engineering and Technology, Karaikudi, Tamilnadu, India, in 2004 and 2008, respectively. He completed PG Dipp VLSI and MBA (Human

Resource Management) in Annamalai University in the year 2009 and 2010, respectively. He completed his Doctoral Degree in Department of Electronics Engineering, School of Engineering and Technology, Pondicherry University, Puducherry, in 2013. He is currently working as Associate Professor, Department of Electronics and Communication Engineering, Mount Zion College of Engineering and Technol-

ogy, Pudukkottai, Tamilnadu, India. He has published more than 25 papers in International Journals and presented more than 50 papers in Inter-national and National Conferences in India and foreign countries. He published two book chapters. He is the reviewer around ten referred journals like IEEE, SPIE, Elsevier, Springer, PIER and HJEEE Journals. He is a life member of ISTE, IETE, CSI, IE(I) and member of IEEE. He attended 35 workshops and organized 14 programmes. His current research interests are in the areas of Optical Communication, Photonic Crystals, Photonic Integrated Circuits, Optical Devices, Microwave communication, Microwave Devices and Optical Networks.